Disorganization of basement membrane zone architecture causes impaired melanocyte inhabitation in vitiligo

Fei Yang [1,2§], Lingli Yang [1§*], Yasutaka Kuroda [1,2], Sylvia Lai [1], Yoshito Takahashi [2], Tetsuya Sayo [2*], Takeshi Namiki [3], Kimiko Nakajima [4], Shigetoshi Sano [4], Shintaro Inoue [5], Daisuke Tsuruta [6] and Ichiro Katayama [1]

[1] Department of Pigmentation Research and Therapeutics, Graduate School of Medicine, Osaka Metropolitan University, Osaka 5450051, Japan

[2] Biological Science Research Laboratories, Kao Corporation, Odawara 2500002, Japan

[3] Department of Dermatology, Tokyo Medical and Dental University Graduate School and Faculty of Medicine, Tokyo 1138510, Japan

[4] Department of Dermatology, Kochi Medical School, Kochi University, Kochi 7838505, Japan

[5] Department of Cosmetic Health Science, Gifu Pharmaceutical University, Gifu 5011196, Japan

[6] Department of Dermatology, Graduate School of Medicine, Osaka Metropolitan University, Osaka 5458585, Japan

[§] These two authors contributed equally to this work: Fei Yang, Lingli Yang.

[*] Correspondence: yang.lingli@omu.ac.jp (L.Y.); sayou.tetsuya@kao.com (T.S.); Tel./Fax: +81-6-6556-7618 (L.Y.); Tel./Fax: +81-465-34-6111 (T.S.)

Keywords: fibroblasts; melanocyte; basement membrane; vitiligo; MMP2

Abbreviations: BM, basement membrane; BMZ, basement membrane zone; MMP2-Fb, MMP2-overexpressing fibroblasts; MMP2, matrix metalloproteinase 2.

Abstract

Vitiligo, a chronic autoimmune skin disorder characterized by selective epidermal melanocyte loss, lacks a well-defined mechanism for this phenomenon. Our study offers compelling insights into vitiligo pathogenesis by revealing disruptions in the basement membrane zone (BMZ) architecture. We observed branched, fragmented, and multilayered lamina densa, accompanied by elevated dermal fibroblast numbers and notable matrix metalloproteinase 2 (MMP2) overexpression. Vitiliginous skin extracts exhibited significant active MMP2 upregulation. To establish a direct link, we intradermally injected MMP2-overexpressing fibroblasts into K14-SCF transgenic mice, resulting in vitiligo-like skin and melanocyte loss, effectively reversed by coadministering MMP2 inhibitors. These groundbreaking findings highlight the pivotal role of disorganized BMZ in vitiligo, proposing MMP2 overexpression in dermal fibroblasts as a potential key contributor. Enhancing our understanding of vitiligo's mechanisms, this research opens avenues for innovative therapeutic strategies against this challenging autoimmune skin disorder.

Teaser

Disrupted skin architecture and MMP2 in dermal fibroblasts hold the key to a potential breakthrough against this puzzling autoimmune disease vitiligo.

Introductions

Vitiligo, an enigmatic skin disorder with a historical record spanning over 3,500 years, currently impacts 1 to 2% of the global population(*1, 2*), characterized by distinct white patches that can appear localized or disseminated white macules(*3*). Rooted in complexities of genetics, oxidative stress, inflammation, and environmental factors, this acquired, idiopathic, autoimmune cutaneous condition has intrigued researchers for generations. Amidst this intricate interplay, one pivotal question arises: How does the delicate interplay between genetics, environmental stressors, and the immune system give rise to the selective disappearance of epidermal melanocytes, leaving these intriguing white macules in its wake(*4, 5*)? While the role of autoreactive $CD8^+$ T cells has been explored in melanocyte destruction(*4, 6*), a deeper exploration into the involvement of other cutaneous cells and the intricacies of the microenvironment surrounding melanocytes in mediating this autoimmune-driven loss continues to elude us.

Under normal homeostatic conditions, epidermal melanocytes, derived from the neural crest, exhibit unique properties, residing in the basal layer of the epidermis in a quiescent state and maintaining a stable ratio with basal keratinocytes(*7*). Perturbations in this delicate balance can lead to intriguing pigmentary disorders(7, 8). The intricate regulation of melanocyte homeostasis involves epidermal keratinocytes, the surrounding stroma, and nearby dermal cells(*9*), with differentiated melanocytes strictly localized at the basement membrane (BM) and reliant on adherence to the basal layers. The

59 BM, a specialized extracellular matrix between the epidermis and dermis(*10, 11*), plays a pivotal role
60 in cellular functions such as adhesion, proliferation, differentiation, and survival(*12*). Despite its well-
61 documented significance in other conditions(*13*) (*14*) (*15*), research on abnormal BM morphology in
62 vitiligo remains limited(*16-19*). Considering the BM's crucial support for keratinocytes and
63 melanocytes, structural abnormalities within the BM could potentially influence melanocyte
64 disappearance in vitiligo. Central to the constitution of the BM is Collagen IV, the most abundant
65 component, serving as its foundational backbone, complemented by laminin, the BM's second most
66 abundant component(*20*), synthesized by keratinocytes and fibroblasts. These matrix proteins form a
67 cohesive and sheet-like BM complex(*20*), enabling basal keratinocytes to establish steadfast
68 connections through hemidesmosomes and focal adhesions(*20*).

69 Matrix metalloproteinases (MMPs), a diverse group of proteolytic enzymes, play a critical role in
70 regulating the cell matrix composition and are essential for various physiological processes(*21*).
71 Dysregulated MMP expression can lead to a wide array of pathological conditions, including
72 inflammation, arthritis, cardiovascular diseases, neurological disorders, and even cancer(*21, 22*).
73 Notably, elevated MMP levels are observed in various autoimmune disorders(*23*) (*24, 25*) (*26*) (*27*)
74 (*28*), indicating their potential involvement in vitiligo.

75 Building upon this knowledge, our comprehensive investigation, employing electron microscopy,
76 three-dimensional/organotypic culture, and mouse experiments, has unveiled a novel mechanism

behind melanocyte disappearance from the BM in vitiligo. The meticulous analysis of lesional skin from vitiligo patients revealed significant aberrations in the BM's structure and components compared to healthy skin, with fibroblast mediated MMP2 overexpression implicated as a key factor leading to BM matrix degradation and subsequent melanocyte detachment. Our findings mark a meaningful milestone in vitiligo research, offering deeper insights into the disease's etiology and pathogenesis.

Results

Basement membrane zone architecture is disorganized in vitiligo

To investigate the BM zone (BMZ) in vitiligo, we performed an ultrastructural analysis using biopsy specimens from both healthy donors (n = 5) and patients with generalized vitiligo (two stable and three progressive cases). We observed abnormal BM morphology in samples from both stable and progressive vitiligo patients. Specifically, healthy skin displayed intact lamina densa with high electron density, while vitiliginous skin showed branched and fragmented lamina densa, some of which were multilayered. the BM of healthy skin contained intact lamina densa with high electron density, whereas the BM of vitiliginous skin contained branched and fragmented lamina densa, some of which were multilayered (**Fig 1a**). Moreover, the anchoring fibrils, which were normally distributed in healthy skin, were scattered and distributed in both the upper and lower portions of the branched lamina densa in vitiliginous skin (**Fig 1a, red asterisks**).

Next, we used immunofluorescence staining to investigate the expression and localization of BM proteins. The BM in healthy skin exhibited normal morphology with a thin continuous linear band of collagen IV and a normal number and distribution of melanocytes. In contrast, vitiliginous skin displayed various abnormal BM morphologies, including obvious thickening, severe disruption, and multilayering, accompanied by the disappearance of melanocytes (**Fig 1b**).

We further investigated the ultrastructural localization of collagen IV using immunoelectron microscopy. In healthy skin, we observed intact BM with collagen IV-labeled gold-particle (**Fig 1c,**

101 **white arrowhead in left panel**) deposits located close to the lamina densa in a continuous
102 arrangement. However, in vitiliginous skin, we observed conspicuous structural alterations of the BM,
103 with collagen IV-labeled gold-particle deposits scattered across a wide area not only close to the
104 normal lamina densa area (**Fig 1c, white arrowhead in right panel**) but also near the branched (**Fig**
105 **1c, white arrow**) and multilayered structures (**Fig 1c, white asterisk**) of lamina densa. These results
106 revealed a disrupted BMZ architecture in lesional vitiliginous skin.

107 **Matrix metalloproteinase 2 expression is elevated in the dermis of vitiliginous skin**

108 To investigate the cause of BM structure disruption, we measured the expression levels of MMP2
109 and MMP9, the major proteolytic enzymes capable of degrading BM collagen, in skin sections from
110 vitiligo patients. We found that vitiliginous skin displayed significantly elevated MMP2 expression in
111 the upper dermis (**Fig 2a and 2b**).

112 Fibroblasts(*29*) and vascular endothelial cells(*30*) are the primary sources of MMP2 production in
113 human skin. To identify the main contributors to elevated MMP2 levels in vitiliginous skin, we
114 conducted immunolocalization studies on healthy and vitiligo-affected skin tissues. Frozen sections
115 from five healthy controls and 11 vitiligo patients were stained with anti-MMP2 antibodies, along with
116 anti-HSP47 (fibroblast marker) and anti-CD31 (endothelial cell marker) antibodies.

117 In the vitiliginous skin, fibroblast numbers were significantly higher compared to healthy skin,
118 while endothelial cell numbers showed no significant difference (**Fig 2c and 2d**). Moreover, MMP2-

119 positive fibroblasts in vitiliginous skin were nearly four times more abundant than in healthy skin,
120 with no significant difference in MMP2-positive endothelial cells (**Fig 2e and 2f**).

121 To investigate MMP2-positive fibroblasts' localization in relation to the BM, we conducted
122 immunofluorescent labeling using anti-MMP2 antibodies, and co-stained with anti-HSP47 and anti-
123 collagen IV (a BM marker) antibodies. Interestingly, MMP2-positive fibroblasts in vitiliginous skin
124 were found in proximity to the BM (**white arrowheads in Fig 2g**) and were observed traversing the
125 BM to reach the epidermis (**white arrows in Fig 2g**).

126 Next, we examined the activity of MMP2 by western blot using skin lysates from three patients
127 with vitiligo (one stable, two progressive) and three healthy controls. MMP2 was highly expressed
128 and mainly in its active form in vitiliginous skin, in contrast to healthy skin where it was slightly
129 expressed and mainly in the inactive form (**Fig 2h and 2i**). These findings indicated that increased
130 MMP2 expression by dermal fibroblasts in vitiliginous skin may contribute to BM destruction and
131 subsequently, melanocyte disappearance.

132 Overexpression of MMP2 in dermal fibroblasts results in melanocyte disappearance

133 To determine whether damage to the BM precedes melanocyte disappearance, we developed an *in*
134 *vitro* 3D skin equivalent model. In this model, half of the collagen gel in the dermis layer was prepared
135 with mock-transfected fibroblasts (Mock-Fbs) and half with MMP2-overexpressing fibroblasts
136 (MMP2-Fbs) (**Fig 3a**). Once the structured collagen gel was established, melanocytes and

137 keratinocytes were uniformly seeded on top of the gel. After 1 week of air-lift culture, macroscopically
138 pigmented skin developed on the part of the gel prepared with Mock-Fbs, whereas no pigmentation
139 developed on the part of the gel prepared with MMP2-Fbs (**Fig 3b**). The 3D skin equivalents prepared
140 with MMP2-Fbs displayed damaged BM and a lack of melanocytes, while those prepared with Mock-
141 Fbs had a typical BM morphology and distributed melanocytes in the basal layer (**Fig 3c**).

142 We further created an *ex vivo* subcutaneous injection model, in which Mock-Fbs or MMP2-Fbs
143 were subcutaneously inoculated into cultured, full-thickness, fresh skin explants. To track the injected
144 fibroblasts, we labeled them with PKH fluorescence cell-membrane labeling dye (**Fig 3d**). Skin
145 explants injected with MMP2-overexpressing fibroblasts displayed BM disruption and melanocyte
146 disappearance (**Fig 3e**). These results indicated that increased MMP2 expression by dermal fibroblasts
147 is a key factor in melanocyte disappearance in vitiligo.

148 **Melanocyte disappearance results from decreased adhesion to the BM**

149 We performed immunofluorescent staining to further examine the disappearance of melanocytes
150 from the damaged BM. Immunofluorescent staining revealed that melanocytes in depigmented 3D
151 skin equivalents tended to be located at the suprabasal layer, detached from the BM, and were negative
152 for cleaved-caspase 3, suggesting that apoptotic events were not involved in their disappearance (**Fig**
153 **4a**).

154 Cells in the basal layer of the epidermis are bound to the BM mainly through integrins, but the

155 mechanistic details of melanocyte adhesion to the BM are still unknown. Melanocytes have been
156 reported to express integrin β1 both *in vitro* and *in vivo(31)*. In addition, discoidin domain receptor 1
157 (DDR1), a membrane protein, was recently reported to bind collagen IV and mediate the adhesion of
158 melanocytes to BM(*32*). Furthermore, some studies reported that loss of melanocytes in vitiligo
159 resulted from decreased DDR1 expression in melanocytes(*33, 34*). We examined adhesion patterns
160 between melanocytes and the BM matrix using *in situ* proximity ligation assay (PLA), an antibody-
161 based technology that enables the visualization of protein–protein interactions. Specifically, we
162 examined integrin β1–laminin-binding and DDR1–collagen IV binding in 3D skin equivalents. In the
163 PLA, when a pair of specific primary antibodies (DDR1 and collagen IV; integrin β1 and laminin) is
164 in close proximity, complementary DNA strands on a corresponding pair of secondary antibodies with
165 PLA probes engage in rolling circle amplification and generate a single fluorescent signal *in situ*,
166 indicating the presence of the corresponding protein–protein interaction (**Fig 4b**). This assay revealed
167 decreased interactions of DDR1–collagen IV and integrin β1–laminin in 3D skin equivalents prepared
168 with MMP2-overexpressing fibroblasts (**Fig 4c and 4d**). Abnormal adhesion between melanocytes
169 and the BM was implicated in their disappearance.

170 Immunofluorescence staining detected melanocyte detachment from the BM in perilesional skin of
171 vitiligo patients (**Fig 5a**). Expression levels of DDR1, collagen IV, integrin β1, and laminin showed
172 no significant difference between healthy and perilesional vitiliginous skin (**Fig 5b, 5c, and 5f**). We

173 employed *in situ* PLA and co-immunohistochemistry staining of melanocytes with anti-TRP1 antibody
174 to visualize adhesions between melanocytes and the BM matrix (**Fig 5d and 5e, white rectangle box**
175 **in lower right panel**). In healthy skin melanocytes, integrin β1–laminin interactions were more
176 predominant compared to DDR1–collagen IV interactions. However, both interactions were
177 significantly diminished in perilesional vitiliginous skin melanocytes (**Fig 5e and 5g**). These findings
178 suggest that melanocyte loss in vitiligo may be linked to a reduced adhesion pattern between
179 melanocytes and the BM (**Fig 5h**).

180 Unlike melanocyte detachment, keratinocyte detachment (blistering) was not observed in
181 depigmented 3D skin equivalents and perilesional vitiliginous skin, despite weakened focal adhesion
182 signal (integrin β1–laminin binding) around basal keratinocytes (**Fig 4c; Fig 5e**). Hence, we
183 investigated hemidesmosome protein expression and binding signals. Expression levels of integrin α6
184 and laminin showed no difference between healthy and lesional vitiliginous skin **(Fig 6a and 6c)**.
185 However, collagen XVII and collagen IV levels were significantly elevated in the lesional vitiliginous
186 skin (**6b and 6c**). Using *in situ* PLA, we examined hemidesmosome adhesion signals between basal
187 keratinocytes and the BM matrix (**Fig 6d**). In healthy skin basal keratinocytes, integrin α6–laminin
188 interactions predominated over collagen XVII–collagen IV interactions (**Fig 6e and 6f**). In contrast,
189 basal keratinocytes of vitiliginous skin exhibited a marked reduction in integrin α6–laminin interaction,
190 while collagen XVII–collagen IV interaction notably increased (**Fig 6e and 6f**). These results suggest

191 altered adhesion patterns between basal keratinocytes and the BM (**Fig 6g**). Compensatory enhanced
192 hemidesmosome adhesion, possibly facilitated by collagen XVII binding to collagen IV, may underlie
193 the absence of skin blistering.

194 **Decreased melanocyte adhesion to the BM is caused by abnormal BM architecture**

195 The expression levels of DDR1, collagen IV, integrin β1, and laminin were similar between
196 vitiliginous and healthy skin. However, vitiliginous skin exhibited decreased DDR1–collagen IV and
197 integrin β1–laminin interactions (**Fig 5**). To investigate the cause of these reduced interactions, we
198 assessed the physical distance between melanocytes and the BM using electron microscopy (**Fig 7a**).
199 As basal cells typically attach to the lamina densa of the BM, we measured the width of the lamina
200 lucida (the distance between the basal cell plasma membrane and the lamina densa) in both healthy
201 and vitiliginous skin. Surprisingly, we found no difference between the two (**Fig 7a and 7c**).

202 To further explore the decreased binding, we performed immunoelectron microscopy. In healthy
203 skin, laminin, the primary adhesion molecule responsible for melanocyte binding to the BM, was
204 clearly distributed along and confined to the lamina densa. However, in lesional and perilesional
205 vitiliginous skin, laminin was diffusely spread within the lamina densa and beneath the disorganized
206 BM architecture (**Fig 7b**). Moreover, the amount of laminin confined in the lamina lucida was
207 significantly reduced in vitiliginous skin compared to healthy skin (**Fig 7b and 7d**). These findings
208 suggest that the disorganized arrangement of the basement membrane zone (BMZ) may contribute to

209 the loss of melanocytes, which rely on laminin for anchoring through the integrin β1 protein.

210 **Inhibition of MMP2 reversed depigmentation in a novel mouse model of vitiligo**

211 Finally, we ultilized K14-SCF transgenic mice, characterized by retained melanocytes in the

212 epidermis, to investigate the impact of BM degradation on skin pigmentation. Murine Mock-Fbs and

213 MMP2-Fbs were subcutaneously transplanted into the back skin of K14-SCF mice (**Fig 8a**).

214 Subcutaneous transplantation of MMP2-Fbs in these mice resulted in vitiligo-like depigmentation (**Fig**

215 **8b**), with disrupted BM structure and absence of epidermal melanocytes (**Fig 8c**). Co-injection of

216 MMP2-Fbs with MMP2 inhibitors (SB-3CT or tanomastat) effectively reversed the depigmentation

217 (**Fig 8d, 8e and 8f**), supporting the crucial role of MMP2 in BM disruption and melanocyte loss. These

218 findings establish the K14-SCF mouse model as a valuable tool for studying vitiligo pathogenesis and

219 highlight MMP2 inhibition as a potential therapeutic approach for vitiligo treatment.

Discussion

The morphological abnormalities of the BM in vitiliginous skin have been previously reported, with thickening(*16, 17*), damage(*18*), or branching(*19*) observed. However, the underlying mechanisms of BM disruption and its role in the pathophysiology of vitiligo have remained unclear. In this study, we confirmed the abnormal BM structure in vitiliginous skin and identified that the disorganized BMZ prevents melanocytes from adhering to the BM via integrin β1–laminin binding. Furthermore, we discovered that the disorganized BM architecture is caused by increased MMP2 expression in dermal fibroblasts. Our findings shed light on the mechanisms underlying melanocyte disappearance in vitiligo and provide insights into potential therapeutic targets.

Previous studies have described melanocyte detachment in vitiligo, but they mostly focused on melanocyte–keratinocyte adhesion(*35, 36*). We addressed this gap by investigating melanocyte–BM adhesion and verified melanocyte detachment in vitiligo. Unlike previous studies that reported decreased expression of adhesion molecules or the melanocyte–BM adhesion molecule DDR1, our *in situ* PLA study revealed that the reduction in melanocyte adhesion was primarily due to the disorganization of the BMZ architecture. Our results suggest that the structural abnormality of the BM, rather than altered expression levels of adhesion molecules, is the primary cause of decreased melanocyte adhesion in vitiligo.

MMP2 and MMP9 are the main MMPs involved in breaking down BM components(*22, 37*). Our

238 study found that MMP2 was dramatically elevated in the dermis of vitiliginous skin, and MMP9
239 expression was slightly increased as well, regardless of whether the vitiligo was stable or progressive.
240 While previous studies have linked decreased E-cadherin expression in melanocytes(*36*) and increased
241 MMP9 expression in vitiliginous skin(*38*) to melanocyte detachment, our findings demonstrate that
242 the detachment of melanocytes is primarily related to their weak attachment to the disorganized BM,
243 mediated by integrin β1–laminin binding and DDR1–collagen IV binding. This supports the notion
244 that MMP2-induced BM disruption plays a crucial role in melanocyte disappearance in vitiligo.
245 The elevated expression of MMP2 in vitiliginous dermal fibroblasts highlights their potential
246 contribution to vitiligo's pathogenesis. Dermal fibroblasts play a crucial role in skin maintenance and
247 healing, and aberrant behavior of these cells has been noted in vitiliginous skin(*39, 40*) (*41*). Our
248 findings propose that increased MMP2 expression in dermal fibroblasts could disrupt the BM structure,
249 resulting in melanocyte detachment. Cytokines like interleukin (IL)-1β(*42, 43*), IL-6(*42*), tumor
250 necrosis factor (TNF)-α(*43, 44*), and TGF-β(*45, 46*) have been reported to stimulate MMP2 expression.
251 Disruption of the BMZ architecture led to shifts in adhesive molecule expression in basal keratinocytes
252 **(Fig 6)**. Likewise, heightened cytokine levels, including IL-1β, TGF-β1, TNF-α, and IL-6, were
253 observed in vitiliginous skin lesions' epidermis **(Extended Data Fig 1)**. Previous research aligns with
254 our findings, suggesting disruption of the epidermal BM modulates interactions between epidermal
255 keratinocytes and the extracellular matrix(*47*). Additionally, significant BM deterioration in

256 pathological settings has been associated with increased cytokine release from epidermal cells(*47-49*).
257 These cytokines might potentially spur MMP2 expression in dermal fibroblasts *via* paracrine
258 regulation.

259 Hence, we present a proposed vicious cycle (**Fig 9**) where MMP2 instigates the BMZ, prompting
260 changes in keratinocyte behavior. This alteration triggers cytokine release and upregulation of MMP2
261 in fibroblasts, perpetuating an unceasing cycle. This impaired BM repair gives rise to a pathological
262 loop of cytokine and protease secretion, culminating in stable vitiligo, an obstinate skin condition.
263 Local stress and microinflammation might incite this cycle. The NLRP3 and NLRP1 inflammasomes,
264 activated by external triggers, initiate microinflammation and innate immunity, prompting increased
265 cytokine levels like IL-1β, IL-6, and TNF-α in the epidermis(*50, 51*). These cytokines could potentially
266 induce MMP2 expression in dermal fibroblasts, initiating the vitiligo development cycle. Further
267 research is necessary to validate this hypothesis.

268 Skin needling, laser ablation, and combined phototherapies with topical agents like steroids,
269 tacrolimus, and 5-fluorouracil exhibit promising outcomes in stable vitiligo treatment(*52-54*). These
270 methods stimulate the dermis, inducing biological changes in fibroblasts, the BM, and keratinocytes.
271 This disruption in the pathogenic cycle aids BMZ repair. Inhibitors of inflammatory pathways, such
272 as JAK inhibitors, may partially alleviate vitiligo. Restoring the BM appears pivotal for melanocyte
273 repopulation. Targeting MMP2 expression and activation through pharmacologic and molecular

274 interventions holds potential for vitiligo prevention and treatment. Normalizing MMP2 expression is
275 crucial for a lasting cure. Clinical evaluation of MMP2 inhibitors shows promise, yet careful
276 consideration of dosage and administration (e.g., topical application) is vital to minimize side effects
277 and maintain melanocyte balance.

278 In our study, heightened MMP2 expression was evident in protein extracts from vitiligo lesions in
279 comparison to healthy skin. Notably, the prevalent form of MMP2 in these extracts was the active 62-
280 kDa variant, indicating localized activation of the latent (pro) form within the dermis of affected skin.
281 The activation of pro-MMP2 is influenced by various factors, including TIMP-2, MT1-MMP,
282 organomercurials, MMP7, and MMP3(*21*). Additional investigations are necessary to ascertain the
283 potential involvement of these factors in MMP2 activation within vitiliginous skin.

284 In conclusion, our study provides valuable insights into the mechanisms of melanocyte
285 disappearance in vitiligo. Disruption of the BM architecture, primarily caused by increased MMP2
286 expression in dermal fibroblasts, plays a crucial role in melanocyte detachment. These findings open
287 new avenues for potential therapeutic strategies targeting MMP2 and BM repair to treat vitiligo.
288 However, further research is needed to fully understand the complex interactions and mechanisms
289 involved in vitiligo pathogenesis.

Figure Legends

Figure 1. Disorganization of basement membrane zone architecture in vitiligo

a, Representative ultrastructural images of ultrathin sections of skin from five healthy controls and five patients with generalized vitiligo. In the right panel, the areas of epidermis and dermis are represented by Epi and Der, respectively, and the basement membrane zone is indicated by a red line. In the left panel, the area of the white rectangle is shown enlarged at the lower right. Red asterisk: anchoring fibril; Epi: epidermis; Der: dermis; BMZ: basement membrane zone. Scale bars: 2 μm. **b,** Representative immunofluorescence images of skin specimens from five healthy controls and 11 patients with generalized vitiligo stained with anti-collagen IV (green), anti-TRP1 (red), and DAPI (blue). The areas in the white rectangles are shown in the corresponding right panels. Scale bar: 100 μm. **c,** Representative immunoelectron microscopy images of frozen sections stained with anti-collagen IV. White arrowhead: collagen IV-labeled gold-particle deposits close to the lamina densa; White arrow: collagen IV-labeled gold-particle deposits close to the branched structure of lamina densa; White asterisk: collagen IV-labeled gold-particle deposits close to the layered structure of lamina densa. Scale bars: 1 μm.

Figure 2. Matrix metalloproteinase 2 expression is elevated in the dermis of

306 **vitiliginous skin**

307 **a,** Representative immunofluorescence images of frozen sections of skin from five healthy controls
308 and 11 patients with generalized vitiligo. MMP2 is stained green, and MMP9 is stained red. Vitiligo-
309 L: lesional vitiliginous skin. **b,** Quantitation of MMP2 and MMP9 expression by fluorescence intensity
310 measurement. **c,** Representative immunofluorescence staining of MMP2, HSP47, and CD31 in skin
311 from healthy controls and patients with vitiligo. **d,** Quantitation of fibroblast and endothelial cell
312 numbers in healthy and vitiliginous skin. **e,** Quantitation of $MMP2^+$ fibroblast and $MMP2^+$ endothelial
313 cell numbers. **f,** The ratios of $MMP2^+$ fibroblasts among all fibroblasts and $MMP2^+$ endothelial cells
314 among all endothelial cells. **g,** Representative immunofluorescence staining of $MMP2^+$ fibroblasts
315 distributed around the BM. MMP2 is stained red; the fibroblast marker HSP47 is stained green; and
316 collagen IV, the main component of BM, is stained blue. White arrowhead: $MMP2^+$ fibroblasts close
317 to the BM; White arrow: $MMP2^+$ fibroblasts passed through the BM. **h,** Western blot analyses showing
318 expression of the pro and active forms of MMP2 in skin lysates from healthy skin and lesional
319 vitiliginous skin. **i,** Quantitation of active MMP2 and total MMP2 (the total of active and pro MMP2)
320 expression according to western blot data. Nuclei are counterstained in blue with DAPI in **a** and **c**.
321 Scale bars in **a** and **c**: 50 μm. Scale bars in **g**: 20 μm.

322 **Figure 3. Overexpression of MMP2 in dermal fibroblasts results in melanocyte**
323 **disappearance in three-dimensional human full-thickness skin equivalent and**

324 **human *ex vivo* cultured skin explants.**

325 **a,** Schematic flow diagram depicting the reconstructed three-dimensional human skin full-thickness
326 equivalent model. **b,** Macroscopic images of skin equivalents. **c,** Representative immunofluorescence
327 staining of the melanocyte marker TRP1 and the BM marker laminin 332 in skin equivalents. TRP1
328 is stained red, and laminin 332 is stained green. Nuclei are counterstained in blue with DAPI. **d,**
329 Schematic diagram of the human skin explant culture model. **e,** Representative immunofluorescence
330 staining of collagen IV and melan-A in cultured human skin explants. Collagen IV is stained blue, and
331 melan-A is stained green. Intradermally injected fibroblasts are labeled with PKH fluorescent dye in
332 red. The white rectangle outlines the area of melanocytes and BM, and the detail is shown in the
333 corresponding lower panel. Scale bars in **c** and **e**: 50 μm. Data in **b**, **d**, **e**, **f,** and **i** are shown as mean ±
334 standard deviation.

335 **Figure 4. Melanocyte disappearance results from decreased adhesion to the BM in**
336 **the three-dimensional skin equivalent model.**

337 **a,** Representative immunofluorescence staining of TRP1 and cleaved-caspase 3 in three-dimensional
338 skin equivalents. TRP1 is stained green, and cleaved-caspase 3 is stained red. Mock-Fb indicates skin
339 equivalent embedded with mock-transfected fibroblasts; MMP2-Fb (MZ) indicates the marginal zone
340 of skin equivalent embedded with MMP2-overexpressing fibroblasts. Detached melanocytes are
341 shown by white arrows. **b,** Schematic diagram of the proximity ligation assay and melanocyte antibody

342 cocktail immunofluorescence co-staining. **c,** The interactions between DDR1 and collagen IV and
343 between integrin β1 and laminin in skin equivalents are visualized in red fluorescence by proximity
344 ligation assay. Melanocytes are visualized in green. Nuclei are counterstained in blue with DAPI. The
345 areas in the white rectangles are shown at the lower right. **d,** Quantitation of the fluorescence intensity
346 around melanocytes in proximity ligation assays of five skin equivalents. Scale bars in **a** and **c**: 50 μm.
347 Data in **d** are shown as mean ± standard deviation.

348 **Figure 5. Melanocyte disappearance results from decreased adhesion to the BM in**
349 **vitiliginous skin.**

350 **a,** Representative immunofluorescence staining of TRP1 in healthy skin and perilesional vitiliginous
351 skin. TRP1 is stained red. Nuclei are counterstained in blue with DAPI. Detached melanocytes are
352 shown by white arrows. Vitiligo-PL indicates perilesional vitiliginous skin. **b,** Representative
353 immunofluorescence staining of DDR1, collagen IV, and TRP1 in healthy skin and perilesional
354 vitiliginous skin. DDR1 is stained green, collagen IV is stained blue, and TRP1 is stained red. The
355 area in the white rectangle is shown on the lower right. The red lines circling the areas in the enlarged
356 images indicate melanocytes. **c,** Representative immunofluorescence staining of integrin β1, laminin,
357 and TRP1 in healthy skin and perilesional vitiliginous skin. Integrin β1 is stained green, laminin is
358 stained blue, and TRP1 is stained red. The area in the white rectangle is shown on the lower right. **d,**
359 Schematic diagram of the proximity ligation assay and melanocyte antibody cocktail

360 immunofluorescence co-staining. **e,** The interactions between DDR1 and collagen IV and between
361 integrin β1 and laminin are visualized in red fluorescence by proximity ligation assay. Melanocytes
362 are visualized in green. Nuclei are counterstained in blue with DAPI. The area in the white rectangle
363 is shown on the lower right. **f,** Quantitation of the immunofluorescence signal around melanocytes in
364 **b** and **c**. **g,** Quantitation of the fluorescence intensity around melanocytes in proximity ligation assays
365 in **e**. **h,** Illustration of melanocyte–BM adhesion in healthy skin and vitiliginous skin. Scale bars in **a,**
366 **b, c,** and **e**: 50 μm. Data in **f** and **g** are shown as mean ± standard deviation.

367 **Figure 6. Compensatory enhanced hemidesmosome adhesion in the basal**
368 **keratinocytes of vitiliginous skin.**

369 **a,** Representative immunofluorescence staining of integrin α6, laminin, and TRP1 in healthy skin and
370 lesional vitiliginous skin. Integrin α6 is stained green, laminin is stained blue, and TRP1 is stained red.
371 The area in the white rectangle is shown on the lower right. **b,** Representative immunofluorescence
372 staining of collagen XVII, collagen IV, and TRP1 in healthy skin and lesional vitiliginous skin.
373 Collagen XVII is stained green, collagen IV is stained blue, and TRP1 is stained red. The area in the
374 white rectangle is shown on the lower right. **c,** Quantitation of the immunofluorescence signal around
375 basal keratinocytes in **a** and **b**. **d,** Schematic diagram of the proximity ligation assay. **e,** The interactions
376 between integrin α6 and laminin and between collagen XVII and collagen IV are visualized in red
377 fluorescence by proximity ligation assay. Nuclei are counterstained in blue with DAPI. The area in the

378 white rectangle is shown on the lower right. **f,** Quantitation of the fluorescence intensity around basal
379 keratinocytes in the proximity ligation assays in **e**. **g,** Illustration of basal keratinocyte–BM adhesion
380 in healthy skin and vitiliginous skin. Scale bars in **a, b,** and **e**: 50 μm. Data in **c** and **f** are shown as
381 mean ± standard deviation.

382 **Figure 7. The decreased adhesion of melanocytes to the BM is due to abnormal BM**
383 **architecture.**

384 **a,** Representative ultrastructural images of ultrathin sections of skin from five healthy controls and
385 five patients with generalized vitiligo. An enlarged image of the area indicated by the red arrowhead
386 is shown on the lower right. The red double arrow indicates the lamina lucida. Epi: epidermis; Der:
387 dermis. Scale bars: 1 μm. **b,** Representative immunoelectron microscopy images of ultrathin skin
388 sections stained with anti-laminin antibody. The area of the lamina lucida is outlined in yellow. Scale
389 bars: 1 μm. **c,** Quantitation of the width of the lamina lucida in **a**. Three measurements were performed
390 per section. **d,** Quantitation of the ratio of the number of laminin gold particles located at the lamina
391 lucida to the length of the lamina lucida. **e,** Illustration of melanocyte–BM adhesion in healthy skin
392 and vitiliginous skin. Data in **c** and **d** are shown as mean ± standard deviation.

393 **Figure 8. Subcutaneous inoculation of mice with MMP2-overexpressing fibroblasts**

induced a vitiligo phenotype that could be reversed by inhibition of MMP2

a, Schematic diagram of the subcutaneous fibroblast inoculation mouse model. **b,** Macro appearance of the mice at 3 weeks after fibroblast inoculation. The bottom panels show the corresponding threshold binarization images of the back skin of the mice. **c,** Representative immunofluorescence staining of TRP1, HSP47, and collagen IV in mouse skin sections. TRP1 is stained red, HSP47 is stained green, and collagen IV is stained blue. The area in the white rectangle is shown in the corresponding lower panel. Scale bars: 50 μm. **d,** Schematic of the experimental procedure to treat mice with MMP2 inhibitor. **e,** Macroscopic images of the mice at 2 weeks after subcutaneous inoculation. The bottom panels show the corresponding threshold binarization images of the back skin of the mice. **f,** Quantitation of the ratio of depigmentation area on the back skin of the mice. Data in **f** are shown as mean ± standard deviation.

Figure 9. Summary illustration of MMP2-induced melanocyte disappearance in vitiligo.

Schematic representation of normal skin and vitiliginous skin. Melanocytes are located at the basal layer of the epidermis interacting with the BM. In normal skin, laminin is normally distributed on collagen IV. Basal melanocytes attach to the BM mainly by integrin β1–laminin binding. In vitiliginous skin, collagen IV is degraded into fragments by the increased $MMP2^{+}$ dermal fibroblasts, the laminin distribution is disrupted, and it is difficult for basal melanocytes to attach to the BM

412 through integrin β1–laminin binding. Melanocytes detach from the BM and disappear from the

413 epidermis. Although integrin β1–laminin binding and integrin α6–laminin binding are diminished in

414 basal keratinocytes of vitiliginous skin, collagen XVII–collagen IV binding is enhanced as a

415 compensatory mechanism.

Materials & Methods

Human skin specimens

Histo-immunofluorescence staining was performed with frozen biopsy samples obtained from lesional and perilesional skin of well-defined patients with non-segmental vitiligo (n = 13, 7 in progressive state and 4 in stable state) (**Table 1**) and from corresponding sites on healthy donors (n = 5; 2 from the abdomen, 2 from an arm, and 1 from the chest). Three-millimeter punch fresh skin biopsy specimens of lesional skin from confirmed patients with vitiligo (n = 3) and samples from corresponding sites on healthy donors (n = 3) were used for protein extraction. One-millimeter punch skin biopsy specimens of lesional skin from confirmed patients with vitiligo (n = 5) and samples from corresponding sites on healthy donors (n = 5) were used for electron microscopy and immuno-electron microscopy analyses. The progressive state of vitiligo was defined by the development of new lesions or the extension of pre-existing lesions in the last 6 months, and the stable state was defined by no increase in the size of existing lesions and an absence of new lesions in the past 1 year. Written informed consent was obtained from all participants prior to study inclusion. The study was approved by the Medical Ethics Committee of Osaka Metropolitan University (No. 4152).

Fluorescent Immunohistochemistry Staining

Human skin tissue and 3D skin samples embedded in OCT compound (Sakura Fineteck, Tokyo, Japan) were cut into 6-μm sections for immunohistochemistry analyses. After fixation with 4%

434 paraformaldehyde (163-20145, Wako, Osaka, Japan) for 10 min and blocking with 5% BSA for 30
435 min at room temperature, these sections were incubated with 1:100 diluted primary antibodies specific
436 for collagen IV (ab6586, Abcam, Cambridge, MA, USA), TRP1 (SIG-38150, Bio Legend, San Diego,
437 CA, USA), MMP2 (ab86607, Abcam), MMP9 (ab119906, Abcam), HSP47 (ADI-SPA-470, Enzo Life
438 Sciences, Farmingdale, NY, USA), CD31 (M0823, Dako, Santa Clara, CA, USA), laminin 332
439 (ab78286, Abcam), melan-A (SIG-38160, Bio Legend), cleaved-caspase 3 (#9664, Cell Signaling
440 Technology, Danvers, MA, USA), DDR1 (PA5-29284, Thermo Fischer Scientific, Waltham, MA,
441 USA), integrin β1 (ab30388, Abcam), Laminin (ab11575, Abcam), integrin α6 (ab20142, Abcam),
442 and collagen XVII (HPA043673, Sigma-Aldrich, Burlington, MA, USA) and then with the appropriate
443 secondary antibody (Alex Fluor 488/555/647 anti-rabbit IgG, anti-mouse IgG1, anti-mouse IgG2a,
444 anti-mouse IgG2b, or anti-goat IgG; 1:1,000, Invitrogen, Grand Island, NY, USA). Nuclei were
445 counterstained with DAPI (#62248, Thermo Fischer Scientific). Murine skin tissues embedded in OCT
446 compound were cut into 6-μm sections for immunohistochemistry analyses. After fixation and
447 blocking, these sections were incubated with 1:100 diluted primary antibodies specific for TRP1 (SIG-
448 38150, Bio Legend), HSP47 (ADI-SPA-470, Enzo Life Sciences), and collagen IV (ab19808, Abcam),
449 and then with the appropriate secondary antibody (Alex Fluor 488 anti-mouse IgG2b, Alex Fluor 555
450 anti-mouse IgG2a, or Alex Fluor 647 anti-rabbit IgG; 1:1,000, Invitrogen). Slides were observed using
451 an LSM 710 Zeiss confocal laser microscope. Images were captured using Zeiss ZEN 2012 software

452 (Carl Zeiss Inc., Jena, Germany). Counting of positively stained cells and measurement of mean
453 fluorescence intensity were carried out using Image J Software (NIH,
454 http://rsb.info.nih.gov/ij/index.html).

455 **Electron Microscopy**

456 Punch biopsy skin samples (1 mm) were fixed with 2.5% glutaraldehyde in 0.1 M phosphate-
457 buffered saline (PBS) at pH 7.4 for 2 h and then washed overnight with PBS. Samples were then post-
458 fixed in 1% O_sO_4 (157-01141, Wako) in PBS for 1h. After washing with DDW, samples were
459 dehydrated with a graded ethanol series and embedded in EPON (TAAB EPON, 342-2, Nisshin EM,
460 Tokyo, Japan). Ultrathin sections (70–80 nm) were cut and transferred to grids, dual-stained with
461 uranyl acetate and lead citrate, and visualized on an FEI Talos F200C G2 Transmission Electron
462 Microscope (Thermo Fisher Scientific). The width of lamina lucida was measured using Image J
463 Software (NIH, http://rsb.info.nih.gov/ij/index.html).

464 **Pre-Embedding Immunoelectron Microscopy**

465 Pre-embedding gold enhancement immunogold labeling was performed as detailed previously(*55*)
466 with a slight modification. Briefly, skin tissues were fixed in 4% paraformaldehyde (163-20145,
467 Wako) for 30 min at room temperature and embedded in OCT compound. Frozen sections (7 μm) were
468 permeabilized in 0.25% saponin (47036, Sigma-Aldrich) for 30 min and then blocked for 30 min in
469 PBS containing 0.1% saponin, 10% bovine serum albumin (013-25773, Wako), 10% normal goat

470 serum (16210-072, Thermo Fisher Scientific), and 0.1% cold water fish skin gelatin (G7041, Sigma-
471 Aldrich). Samples were incubated with anti-collagen IV (1:100; ab19808, Abcam) or anti-laminin
472 (1:100; ab11575, Abcam) overnight at 4°C in a blocking solution and then with colloidal gold-
473 conjugated anti-rabbit IgG (1.4-nm diameter; 1:200; #2003, Nanoprobes, Yaphank, NY, USA) in a
474 blocking solution for 2 h at room temperature. The signal was intensified with the Gold Enhancement
475 EM Kit (#2113, Nanoprobes) for 4 min at room temperature. The specimens were post-fixed in 1%
476 OsO4, dehydrated in a series of graded ethanol solutions, and embedded in EPON (TAAB EPON,
477 342-2, Nisshin EM). Ultrathin sections (70 nm) were collected and stained with uranyl acetate and
478 lead citrate. Images were taken with an FEI Talos F200C G2 Transmission Electron Microscope
479 (Thermo Fisher Scientific) equipped with an Advanced Microscopy Techniques charge-coupled
480 device-based camera system. The quantitation analyses of positive gold particles were carried out
481 using Image J Software (NIH, http://rsb.info.nih.gov/ij/index.html).

482 **Western Blot Analyses**

483 For the preparation of protein samples, punch fresh skin biopsy specimens were extracted as
484 described previously(*56*). Five micrograms of extracted protein was used for western blot analysis
485 with primary antibody against MMP2 (1:200; ab92536, Abcam). The signal intensity of bands was
486 quantified using the Image J densitometry software (NIH).

487 **Cell Culture and Establishment of MMP2-Overexpressing Cells**

488 Normal human dermal fibroblasts (Neonatal, Primary, FC-0001, Lifeline Cell Technology, Carlsbad,
489 CA, USA) were maintained in MEM (M4655, Sigma-Aldrich) with 1% NEAA (139-15651, Wako),
490 5% FBS (10270-106, Gibco, Thermo Fisher Scientific), 1 mM Sodium Pyruvate (11360-070, Gibco,
491 Thermo Fisher Scientific), and 1% penicillin/streptomycin (168-23191, Wako). C57BL/6 mouse
492 dermal fibroblasts (Neonatal, Primary, SCR-M230057, ScienCell Research Laboratories, Carlsbad,
493 CA, USA) were maintained in Fibroblast Medium-2 (2331, ScienCell Research Laboratories). Cells
494 were incubated at 37°C in a humidified incubator supplied with 5% CO_2.

495 Normal human dermal fibroblasts and C57BL/6 mouse dermal fibroblasts (2×10^6 cells/well on 10-
496 cm plates) were transfected with 20 μg human MMP2 expression or murine MMP2 expression
497 episomal vector DNA or empty episomal vector DNA (customized pEBMulti-Puro, Fujifilm Wako
498 Pure Chemical Corporation, Osaka, Japan) mixed with P3000 and Lipofectamine 3000
499 (Lipofectamine™ 3000, Thermo Fisher Scientific). Successfully transfected cells were selected with
500 1 μg/ml puromycin according to the manufacturer's instructions. The expression of the MMP2 proteins
501 in cell lysate and culture medium were confirmed by western blot analyses using antibody against
502 MMP2 (ab92536, Abcam).

503 **Reconstructed Three-Dimensional Human Full-Thickness Skin Equivalents**

504 A reconstructed 3D human full-thickness skin equivalent model was generated as described

505 previously(*57*) with modification. Collagen gels were prepared from an acid collagen solution (IAC-
506 50, Koken Ltd., Tokyo, Japan) according to the manufacturer's protocol. Then, 2.5×10^5 fibroblasts
507 were cultured on collagen gel in MEM (M4655, Sigma-Aldrich) with 1% NEAA (139-15651, Wako),
508 5% FBS (10270-106, Gibco, Thermo Fisher Scientific), 1 mM sodium pyruvate (11360-070, Gibco,
509 Thermo Fisher Scientific), and 1% penicillin/streptomycin (168-23191, Wako). This medium was
510 changed every other day after fibroblast mounting. Two days after the dermal component was prepared,
511 a cell suspension of 8.4×10^5 keratinocytes and 1.2×10^5 melanocytes in 60 μl medium composed of
512 a 1:1 mixture of Epilife and Medium 254 was seeded onto the concave surface of the contracted gel.
513 After 30 min, 2 ml culture medium was added to the inside and outside of the transwell, and the
514 submerged culture was maintained for 2 days. The culture medium was composed of DMEM/F-12
515 (3:1 vol/vol; D5921, N4888, Sigma-Aldrich) containing 0.3% FCS, 0.1 mM ethanolamine, 0.1 mM *o*-
516 phosphoethanolamine, 0.4 μg/ml hydrocortisone, 5 μg/ml insulin, 0.09 mM adenine, 5 μg/ml
517 transferrin, 20 pM triiodothyronine, 0.64 mM choline chloride, 0.675 mM serine, 20 μg/ml linoleic
518 acid/BSA, 50 μg/ml ascorbic acid, 7.25 mM glutamine, 10 nM progesterone, 100 I.U./ml penicillin,
519 and 100 μg/ml streptomycin. The thus-formed early skin equivalents were then raised to the air-liquid
520 interface and placed in cornification medium composed of a 1:1 mixture of Ham's F-12 and DMEM
521 supplemented with 0.3% FCS, 0.1 mM ethanolamine, 0.1 mM *o*-phosphoethanolamine, 0.4 μg/ml
522 hydrocortisone, 5 μg/ml insulin, 0.09 mM adenine, 5 μg/ml transferrin, 20 pM triiodothyronine, 0.64

523 mM choline chloride, 0.75 mM serine, 20 μg/ml linoleic acid/BSA, 50 μg/ml ascorbic acid, 7.25 mM
524 glutamine, 0.75 mM calcium chloride, 100 I.U./ml penicillin, and 100 μg/ml streptomycin. The
525 medium was subsequently changed every other day. One week after the air-liquid interface incubation,
526 the skin equivalents were harvested and subjected to macroscopic examination and further histology
527 analyses. All skin equivalent experiments were performed in quintuplicate in five transwells.

528 To prepare the half-half 3D human skin equivalent, MMP2-overexpressing fibroblasts embedded in
529 collagen gel were incubated at 37℃ for 30 min. The early-formed dermal tissue construct was then
530 cut into half size and transferred to one side of a culture transwell insert, and freshly prepared collagen
531 solution containing normal fibroblasts was injected into the other side of the transwell insert. After 2
532 days of culture, keratinocytes and melanocytes were seeded as described above.

533 **Ex Vivo Human Skin Explant Culture**

534 Skin from the lateral abdomen was obtained with the informed consent of patients undergoing
535 abdomen reduction surgery, in accordance with the ethical guidelines of the Research Ethics
536 Committee of Osaka Metropolitan University (No. 4152). The explants were cut (1.0 cm^2) and cultured
537 at an air-liquid interface on culture inserts (filter pore size 8 μm; #141082, Thermo Fisher Scientific)
538 with a 1:1 mixture of Ham's F-12 and DMEM supplemented with 0.3% FCS, 0.1 mM ethanolamine,
539 0.1 mM *o*-phosphoethanolamine, 0.4 μg/ml hydrocortisone, 5 μg/ml insulin, 0.09 mM adenine, 5
540 μg/ml transferrin, 20 pM triiodothyronine, 0.64 mM choline chloride, 0.75 mM serine, 20 μg/ml

541 linoleic acid/BSA, 50 μg/ml ascorbic acid, 7.25 mM glutamine, 0.75 mM calcium chloride, 100
542 I.U./ml penicillin, and 100 μg/ml streptomycin. The insert was set on a 12-well plate (3401, Corning
543 Inc., Corning, NY, USA) and cultured at 37℃ in a humidified incubator with 5% CO_2 for 7 days.
544 For fibroblast inoculation, normal fibroblasts and MMP2-overexpressing fibroblasts were labeled
545 with the red fluorescent dye PKH26 (MINI26-1KT, Sigma-Aldrich) according to the manufacturer's
546 instructions and then subcutaneously injected into cultured human skin explants at a density of 5×10^6
547 cells/ml in 100 μl using disposable 35G needles (ReactSystem, Osaka, Japan).

548 ***In Situ* Proximity Ligation Assay**

549 Multicolor *in situ* PLA was performed using the Duolink PLA Multicolor detection kit (Duolink®
550 PLA® Multicolor Reagent Pack, DUO96000, Sigma-Aldrich) as described previously(*58*) with slight
551 modification. Briefly, frozen skin sections were blocked with blocking solution (DUO82007, Duolink,
552 Sigma-Aldrich) for 30 min at 37 °C and then incubated overnight at 4°C with primary antibodies pre-
553 conjugated with Red Oligo A (DUO86010A, Sigma-Aldrich) or Red Oligo B (DUO86010B, Sigma-
554 Aldrich). After washing with Duolink *In Situ* Wash Buffer A (DUO82046, Sigma-Aldrich), ligation
555 and amplification reactions were performed using a Duolink PLA Multicolor detection kit (DUO96000,
556 Sigma-Aldrich).
557 For co-staining with melanocyte marker after amplification and washing, sections were incubated
558 with the Alexa Fluor 488-conjugated antibody cocktail (MART1 + Tyrosinase + gp100) [Alexa Fluor®

559 488] (1:100 dilution; NBP2-34681AF488, Novus Biologics, San Jose, CA, USA) for 2 h. After 30 min

560 of washing with Duolink *In Situ* Wash Buffer B (DUO82048, Sigma-Aldrich), sections were mounted

561 using Duolink *In Situ* Mounting Medium with DAPI (DUO82040, Sigma-Aldrich). Then, slides were

562 observed using an LSM 710 Zeiss confocal laser microscope. Images were captured using Zeiss ZEN

563 2012 software (Carl Zeiss Inc., Jena, Germany). Mean fluorescence intensity measurements were

564 carried out using Image J Software (NIH, http://rsb.info.nih.gov/ij/index.html).

565 **Animals and *In Vivo* Experimental Procedures**

566 Krt14-Kitl mice, a C57BL/6-background congenic strain that expresses membrane-bound stem

567 cell factor under the keratin14 promoter to retain epidermal melanocytes and thus have pigmented

568 skin, were purchased from the RIKEN BioResource Research Center (No. RBRC00694, RIKEN BRC,

569 Tsukuba, Ibaraki, Japan). PBS, Mock-Fbs, or MMP2-Fbs (5×10^6 cells/ml in 100 μl PBS) was

570 subcutaneously injected into the back skin of male 7-week-old Krt14-Kitl mice.

571 For treatment, 5 μM SB-3CT dissolved in DMSO (HY-12354, MedChemExpress, Monmouth

572 junction, NJ, USA) or 5 μM Tanomastat dissolved in DMSO (T006900, Toronto Research Chemicals,

573 Toronto, Canada) was subcutaneously co-injected with Mock-Fbs or MMP2-Fbs (5×10^6/ml in 100

574 μl PBS) into the back skin of Krt14-Kitl mice. Two weeks after these treatments, the back skin of the

575 mice was depilated and photographed, and the depigmentation area (n = 5 mice per group) was

576 measured using binarization and different global thresholding values (Image J Software, NIH,

http://rsb.info.nih.gov/ij/index.html). Experiments were conducted in accordance with the Guiding Principles for the Care and Use of Laboratory Animals, and the experimental protocol used in this study was approved by the Committee for Animal Experiments at Osaka Metropolitan University (Permit No. 18042, Osaka, Japan).

Statistical Analysis

Experiments were repeated at least three times. Data are presented as the mean ± standard deviation. One-way analysis of variance with Dunnet's test or unpaired Student's t-test (two-tailed) was used for statistical analyses. A value of $p < 0.05$ indicated statistical significance. All statistical analyses for this study were performed using GraphPad Prism version 8.0.0 for Windows (GraphPad Software Inc., San Diego, CA, USA).

Table 1. Clinical characteristics of the patients.

Patient No.	Sex	Age (years)	Type	Biopsy site	Activity
1[§]	M	72	Non-segmental vitiligo	Back	Progressive
2[§]	F	49	Non-segmental vitiligo	Lumbar	Stable
3[*]	M	44	Non-segmental vitiligo	Back	Progressive
4[*]	F	33	Non-segmental vitiligo	Axilla	Progressive
5[*]	F	71	Non-segmental vitiligo	Elbow	Stable
6[§]	F	23	Non-segmental vitiligo	Abdomen	Stable
7[§]	M	30	Non-segmental vitiligo	Lateral abdomen	Progressive
8[§]	F	20	Non-segmental vitiligo	Abdomen	Progressive
9	M	68	Non-segmental vitiligo	Back	Progressive
10	F	49	Non-segmental vitiligo	Abdomen	Progressive
11	F	62	Non-segmental vitiligo	Neck	Stable

*Samples for full skin protein extract were obtained from these three patients.

[§]Samples for electron microscopy were from these five patients.

References

1. M. Picardo *et al.*, Vitiligo. *Nat Rev Dis Primers* **1**, 15011 (2015).
2. A. Alikhan, L. M. Felsten, M. Daly, V. Petronic-Rosic, Vitiligo: a comprehensive overview Part I. Introduction, epidemiology, quality of life, diagnosis, differential diagnosis, associations, histopathology, etiology, and work-up. *J Am Acad Dermatol* **65**, 473-491 (2011).
3. I. C. Le Poole, R. M. van den Wijngaard, W. Westerhof, R. P. Dutrieux, P. K. Das, Presence or absence of melanocytes in vitiligo lesions: an immunohistochemical investigation. *J Invest Dermatol* **100**, 816-822 (1993).
4. E. L. Katz, J. E. Harris, Translational Research in Vitiligo. *Front Immunol* **12**, 624517 (2021).
5. A. B. Lerner, Vitiligo. *J Invest Dermatol* **32**, 285-310 (1959).
6. C. Bergqvist, K. Ezzedine, Vitiligo: A Review. *Dermatology* **236**, 571-592 (2020).
7. M. Cichorek, M. Wachulska, A. Stasiewicz, A. Tyminska, Skin melanocytes: biology and development. *Postepy Dermatol Alergol* **30**, 30-41 (2013).
8. N. K. Haass, M. Herlyn, Normal human melanocyte homeostasis as a paradigm for understanding melanoma. *J Investig Dermatol Symp Proc* **10**, 153-163 (2005).
9. A. Santiago-Walker, L. Li, N. K. Haass, M. Herlyn, Melanocytes: from morphology to application. *Skin Pharmacol Physiol* **22**, 114-121 (2009).
10. M. Costell *et al.*, Perlecan maintains the integrity of cartilage and some basement membranes. *J Cell Biol* **147**, 1109-1122 (1999).
11. A. C. Erickson, J. R. Couchman, Still more complexity in mammalian basement membranes. *J Histochem Cytochem* **48**, 1291-1306 (2000).
12. C. Q. Lin, M. J. Bissell, Multi-faceted regulation of cell differentiation by extracellular matrix. *FASEB J* **7**, 737-743 (1993).
13. L. A. Walakovits, V. L. Moore, N. Bhardwaj, G. S. Gallick, M. W. Lark, Detection of stromelysin and collagenase in synovial fluid from patients with rheumatoid arthritis and posttraumatic knee injury. *Arthritis Rheum* **35**, 35-42 (1992).
14. V. Checchi *et al.*, The Role of Matrix Metalloproteinases in Periodontal Disease. *Int J Environ Res Public Health* **17**, (2020).
15. U. K. Saarialho-Kere, S. O. Kovacs, A. P. Pentland, J. E. Olerud, H. G. Welgus, W. C. Parks, Cell-matrix interactions modulate interstitial collagenase expression by human keratinocytes actively involved in wound healing. *J Clin Invest* **92**, 2858-2866 (1993).
16. M. M. Fawzy, Z. M. El Maadawi, R. A. Hegazy, N. S. El Fatah, Vitiligo - The story from within: A transmission electron microscopic study before and after narrow-band

626 ultraviolet B. *Ultrastruct Pathol* **40**, 265-275 (2016).
627 17. L. F. Montes, J. Abulafia, W. H. Wilborn, B. M. Hyde, C. M. Montes, Value of
628 histopathology in vitiligo. *Int J Dermatol* **42**, 57-61 (2003).
629 18. A. L. Panuncio, R. Vignale, Ultrastructural studies in stable vitiligo. *Am J Dermatopathol*
630 **25**, 16-20 (2003).
631 19. A. S. Breathnach, S. Bor, L. M. Wyllie, Electron microscopy of peripheral nerve terminals
632 and marginal melanocytes in vitiligo. *J Invest Dermatol* **47**, 125-140 (1966).
633 20. C. Has, A. Nystrom, Epidermal Basement Membrane in Health and Disease. *Curr Top*
634 *Membr* **76**, 117-170 (2015).
635 21. H. Nagase, J. F. Woessner, Jr., Matrix metalloproteinases. *J Biol Chem* **274**, 21491-21494
636 (1999).
637 22. V. W. Yong, C. A. Krekoski, P. A. Forsyth, R. Bell, D. R. Edwards, Matrix
638 metalloproteinases and diseases of the CNS. *Trends Neurosci* **21**, 75-80 (1998).
639 23. M. Ram, Y. Sherer, Y. Shoenfeld, Matrix metalloproteinase-9 and autoimmune diseases. *J*
640 *Clin Immunol* **26**, 299-307 (2006).
641 24. J. Song *et al.*, Focal MMP-2 and MMP-9 activity at the blood-brain barrier promotes
642 chemokine-induced leukocyte migration. *Cell Rep* **10**, 1040-1054 (2015).
643 25. S. Agrawal *et al.*, Dystroglycan is selectively cleaved at the parenchymal basement
644 membrane at sites of leukocyte extravasation in experimental autoimmune
645 encephalomyelitis. *J Exp Med* **203**, 1007-1019 (2006).
646 26. D. Leppert *et al.*, Matrix metalloproteinase-9 (gelatinase B) is selectively elevated in CSF
647 during relapses and stable phases of multiple sclerosis. *Brain* **121 (Pt 12)**, 2327-2334
648 (1998).
649 27. I. Tchetverikov *et al.*, Matrix metalloproteinases-3, -8, -9 as markers of disease activity
650 and joint damage progression in early rheumatoid arthritis. *Ann Rheum Dis* **62**, 1094-
651 1099 (2003).
652 28. Y. T. Konttinen *et al.*, Matrix metalloproteinase (MMP)-9 type IV collagenase/gelatinase
653 implicated in the pathogenesis of Sjogren's syndrome. *Matrix Biol* **17**, 335-347 (1998).
654 29. T. Kobayashi, S. Hattori, H. Shinkai, Matrix metalloproteinases-2 and -9 are secreted from
655 human fibroblasts. *Acta Derm Venereol* **83**, 105-107 (2003).
656 30. L. Wang *et al.*, Matrix metalloproteinase 2 (MMP2) and MMP9 secreted by
657 erythropoietin-activated endothelial cells promote neural progenitor cell migration. *J*
658 *Neurosci* **26**, 5996-6003 (2006).
659 31. G. Zambruno, P. C. Marchisio, A. Melchiori, S. Bondanza, R. Cancedda, M. De Luca,
660 Expression of integrin receptors and their role in adhesion, spreading and migration of
661 normal human melanocytes. *J Cell Sci* **105 (Pt 1)**, 179-190 (1993).

662 32. M. Fukunaga-Kalabis *et al.*, CCN3 controls 3D spatial localization of melanocytes in the
663 human skin through DDR1. *J Cell Biol* **175**, 563-569 (2006).
664 33. A. S. Ricard *et al.*, Study of CCN3 (NOV) and DDR1 in normal melanocytes and vitiligo
665 skin. *Exp Dermatol* **21**, 411-416 (2012).
666 34. A. Reichert-Faria, J. E. Jung, V. Moreschi Neto, C. C. de Castro, M. T. Mira, L. Noronha,
667 Reduced immunohistochemical expression of Discoidin Domain Receptor 1 (DDR1) in
668 vitiligo skin. *J Eur Acad Dermatol Venereol* **27**, 1057-1059 (2013).
669 35. Y. Gauthier, M. Cario-Andre, S. Lepreux, C. Pain, A. Taieb, Melanocyte detachment after
670 skin friction in non lesional skin of patients with generalized vitiligo. *British Journal of*
671 *Dermatology* **148**, 95-101 (2003).
672 36. R. Y. Wagner *et al.*, Altered E-Cadherin Levels and Distribution in Melanocytes Precede
673 Clinical Manifestations of Vitiligo. *J Invest Dermatol* **135**, 1810-1819 (2015).
674 37. V. M. Kahari, U. Saarialho-Kere, Matrix metalloproteinases and their inhibitors in tumour
675 growth and invasion. *Ann Med* **31**, 34-45 (1999).
676 38. N. Boukhedouni *et al.*, Type-1 cytokines regulate MMP-9 production and E-cadherin
677 disruption to promote melanocyte loss in vitiligo. *JCI Insight* **5**, (2020).
678 39. V. Delmas, L. Larue, Molecular and cellular basis of depigmentation in vitiligo patients.
679 *Exp Dermatol* **28**, 662-666 (2019).
680 40. Z. Xu *et al.*, Anatomically distinct fibroblast subsets determine skin autoimmune patterns.
681 *Nature* **601**, 118-124 (2022).
682 41. D. Kovacs *et al.*, Vitiligo Skin: Exploring the Dermal Compartment. *J Invest Dermatol* **138**,
683 394-404 (2018).
684 42. K. Kusano *et al.*, Regulation of matrix metalloproteinases (MMP-2, -3, -9, and -13) by
685 interleukin-1 and interleukin-6 in mouse calvaria: association of MMP induction with
686 bone resorption. *Endocrinology* **139**, 1338-1345 (1998).
687 43. D. A. Siwik, D. L. Chang, W. S. Colucci, Interleukin-1beta and tumor necrosis factor-
688 alpha decrease collagen synthesis and increase matrix metalloproteinase activity in cardiac
689 fibroblasts in vitro. *Circ Res* **86**, 1259-1265 (2000).
690 44. J. Y. Choi, M. S. Piao, J. B. Lee, J. S. Oh, I. G. Kim, S. C. Lee, Propionibacterium acnes
691 stimulates pro-matrix metalloproteinase-2 expression through tumor necrosis factor-
692 alpha in human dermal fibroblasts. *J Invest Dermatol* **128**, 846-854 (2008).
693 45. C. M. Overall, J. L. Wrana, J. Sodek, Transcriptional and post-transcriptional regulation
694 of 72-kDa gelatinase/type IV collagenase by transforming growth factor-beta 1 in human
695 fibroblasts. Comparisons with collagenase and tissue inhibitor of matrix metalloproteinase
696 gene expression. *J Biol Chem* **266**, 14064-14071 (1991).
697 46. N. Philips, T. Keller, S. Gonzalez, TGF beta-like regulation of matrix metalloproteinases

698 by anti-transforming growth factor-beta, and anti-transforming growth factor-beta 1
699 antibodies in dermal fibroblasts: Implications for wound healing. *Wound Repair Regen* **12**,
700 53-59 (2004).
701 47. E. M. Yazlovitskaya *et al.*, The laminin-binding integrins regulate nuclear factor kappaB-
702 dependent epithelial cell polarity and inflammation. *J Cell Sci* **134**, (2021).
703 48. D. Breitkreutz, I. Koxholt, K. Thiemann, R. Nischt, Skin basement membrane: the
704 foundation of epidermal integrity--BM functions and diverse roles of bridging molecules
705 nidogen and perlecan. *Biomed Res Int* **2013**, 179784 (2013).
706 49. M. C. Ryan *et al.*, The functions of laminins: lessons from in vivo studies. *Matrix Biol* **15**,
707 369-381 (1996).
708 50. J. Marie *et al.*, Inflammasome activation and vitiligo/nonsegmental vitiligo progression.
709 *Br J Dermatol* **170**, 816-823 (2014).
710 51. S. Moretti *et al.*, New insights into the pathogenesis of vitiligo: imbalance of epidermal
711 cytokines at sites of lesions. *Pigment Cell Res* **15**, 87-92 (2002).
712 52. S. A. Elshafy Khashaba, R. A. Elkot, A. M. Ibrahim, Efficacy of NB-UVB, microneedling
713 with triamcinolone acetonide, and a combination of both modalities in the treatment of
714 vitiligo: A comparative study. *J Am Acad Dermatol* **79**, 365-367 (2018).
715 53. W. Bayoumi *et al.*, Effect of a preceding laser dermabrasion on the outcome of combined
716 therapy with narrowband ultraviolet B and potent topical steroids for treating
717 nonsegmental vitiligo in resistant localizations. *Br J Dermatol* **166**, 208-211 (2012).
718 54. K. Ezzedine, V. Eleftheriadou, M. Whitton, N. van Geel, Vitiligo. *Lancet* **386**, 74-84
719 (2015).
720 55. M. Hayashi-Nishino, N. Fujita, T. Noda, A. Yamaguchi, T. Yoshimori, A. Yamamoto, A
721 subdomain of the endoplasmic reticulum forms a cradle for autophagosome formation.
722 *Nat Cell Biol* **11**, 1433-1437 (2009).
723 56. F. Yang, L. Yang, M. Wataya-Kaneda, T. Yoshimura, A. Tanemura, I. Katayama,
724 Uncoupling of ER/Mitochondrial Oxidative Stress in mTORC1 Hyperactivation-
725 Associated Skin Hypopigmentation. *J Invest Dermatol* **138**, 669-678 (2018).
726 57. L. Yang *et al.*, Microbubble-enhanced ultrasound for gene transfer into living skin
727 equivalents. *J Dermatol Sci* **40**, 105-114 (2005).
728 58. C. Phoomak *et al.*, The translocon-associated protein (TRAP) complex regulates quality
729 control of N-linked glycosylation during ER stress. *Sci Adv* **7**, (2021).
730

Figure 1

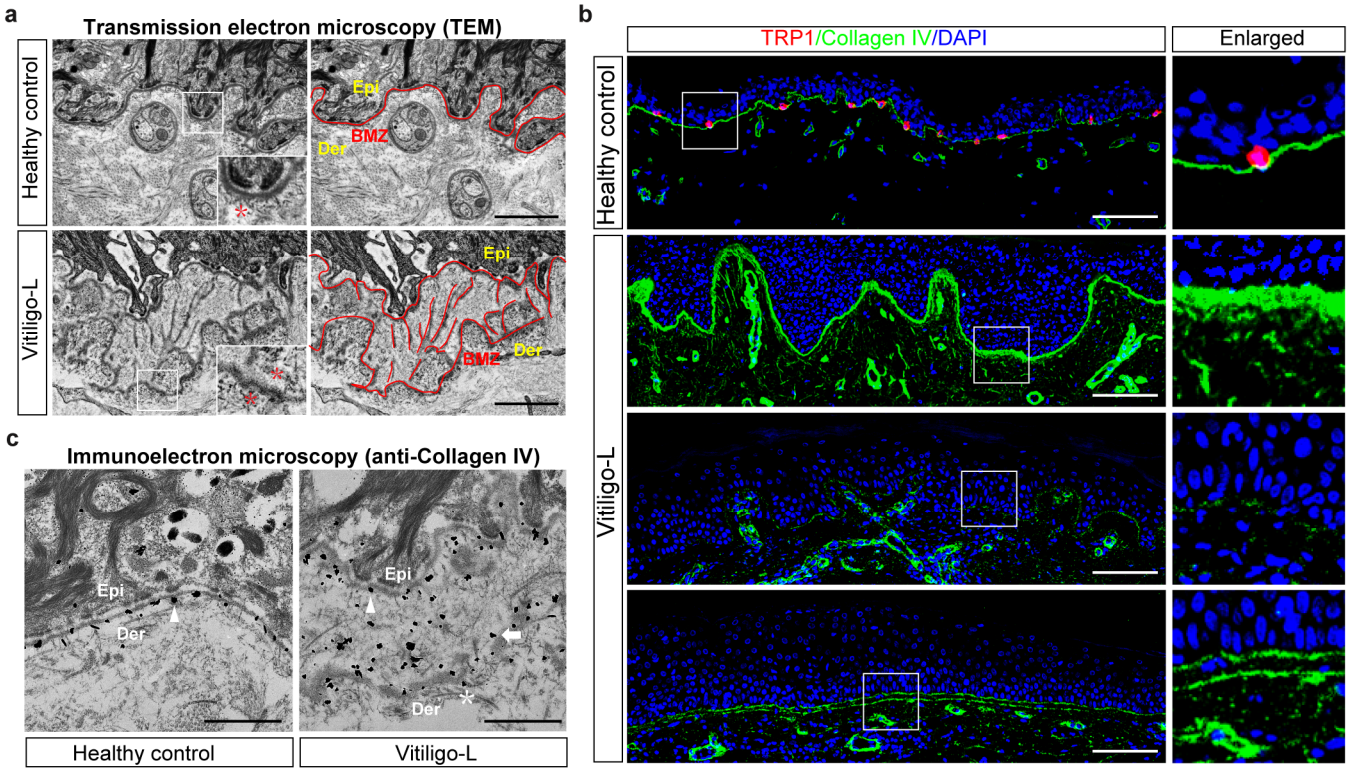

Figure 2

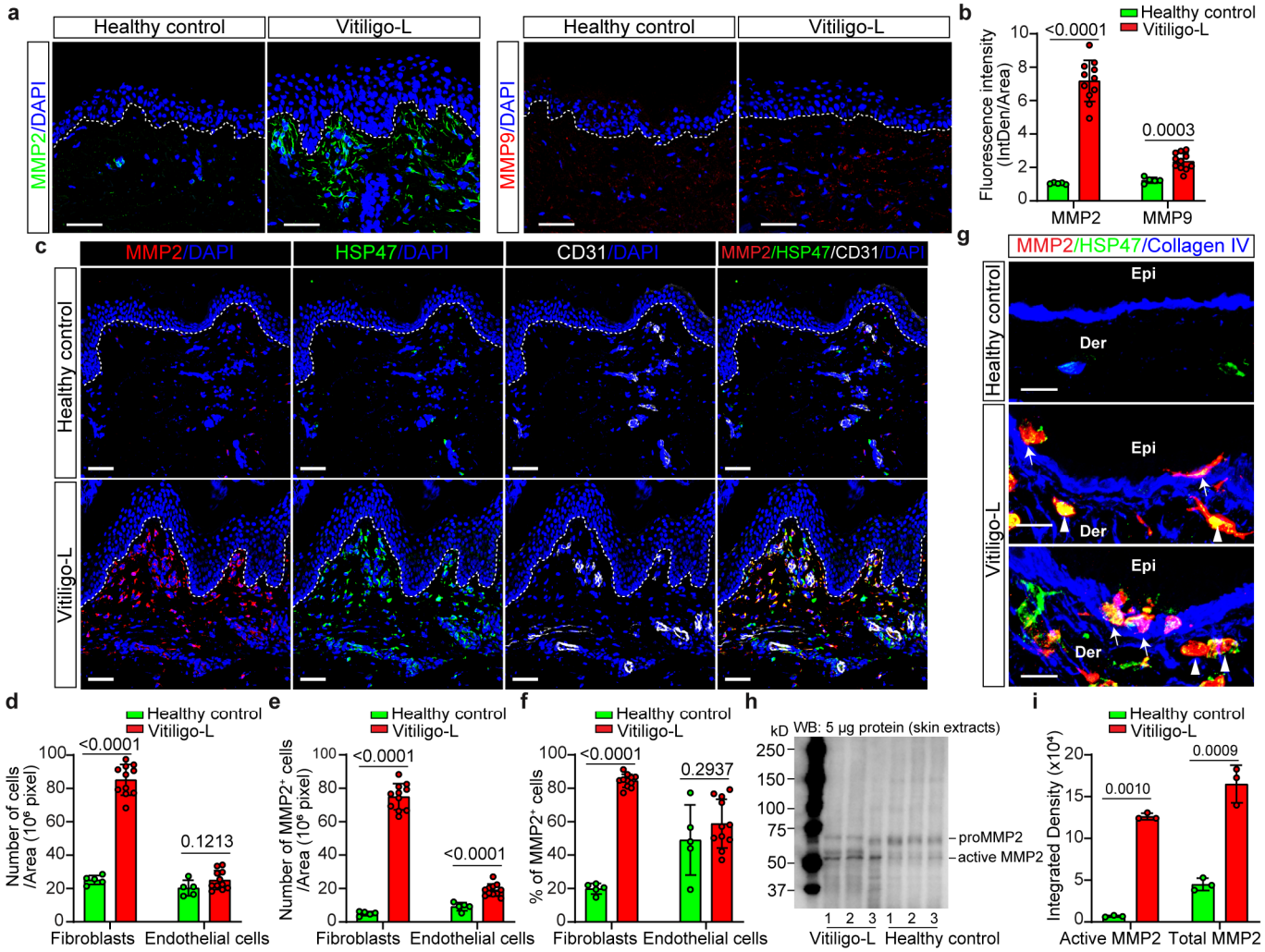

Figure 3

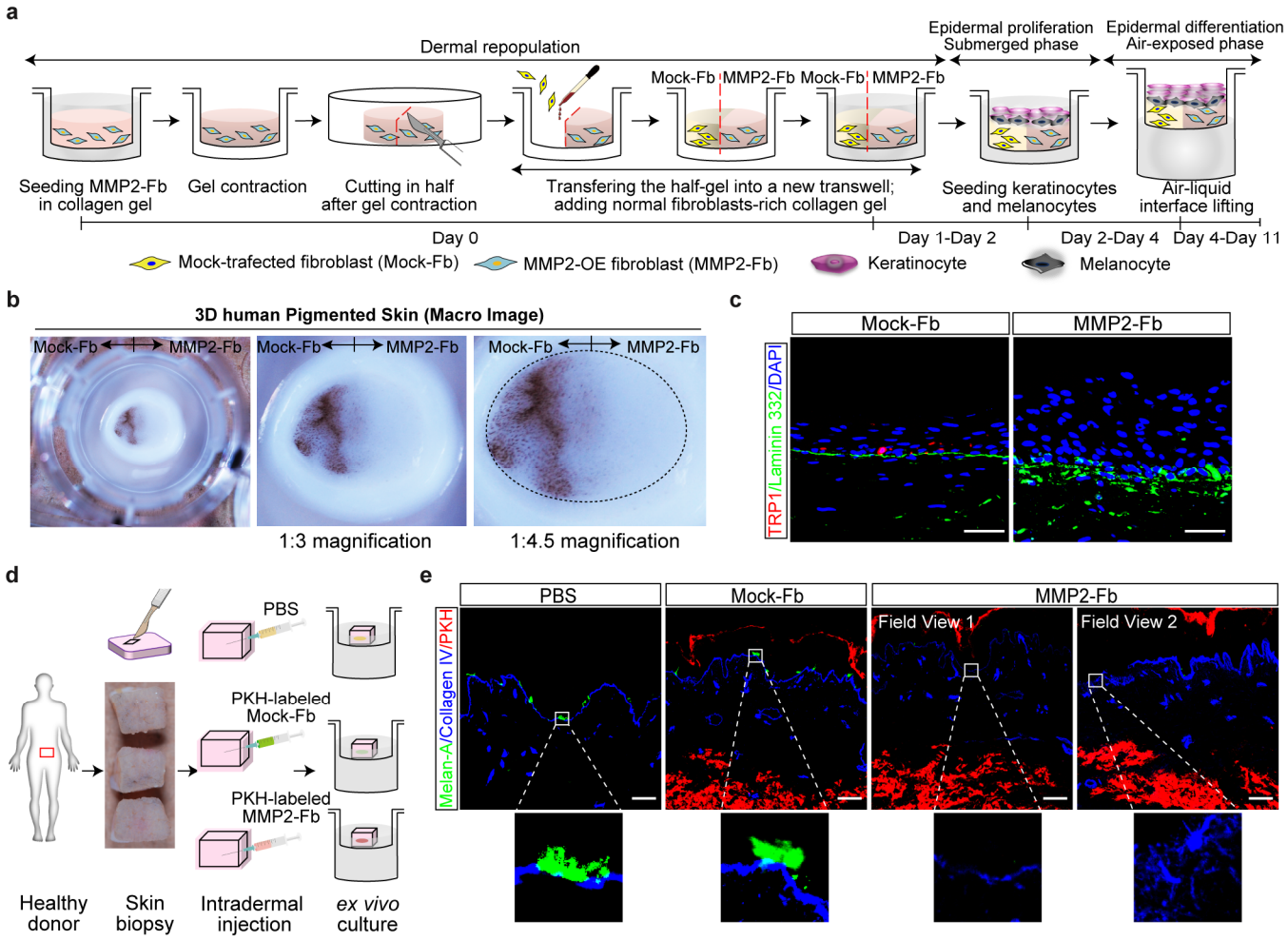

Figure 4

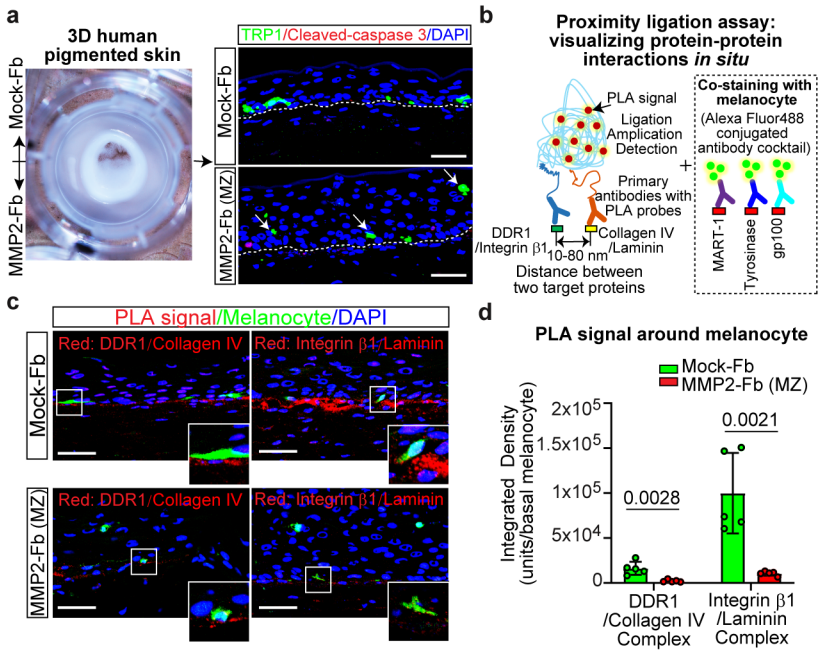

Figure 5

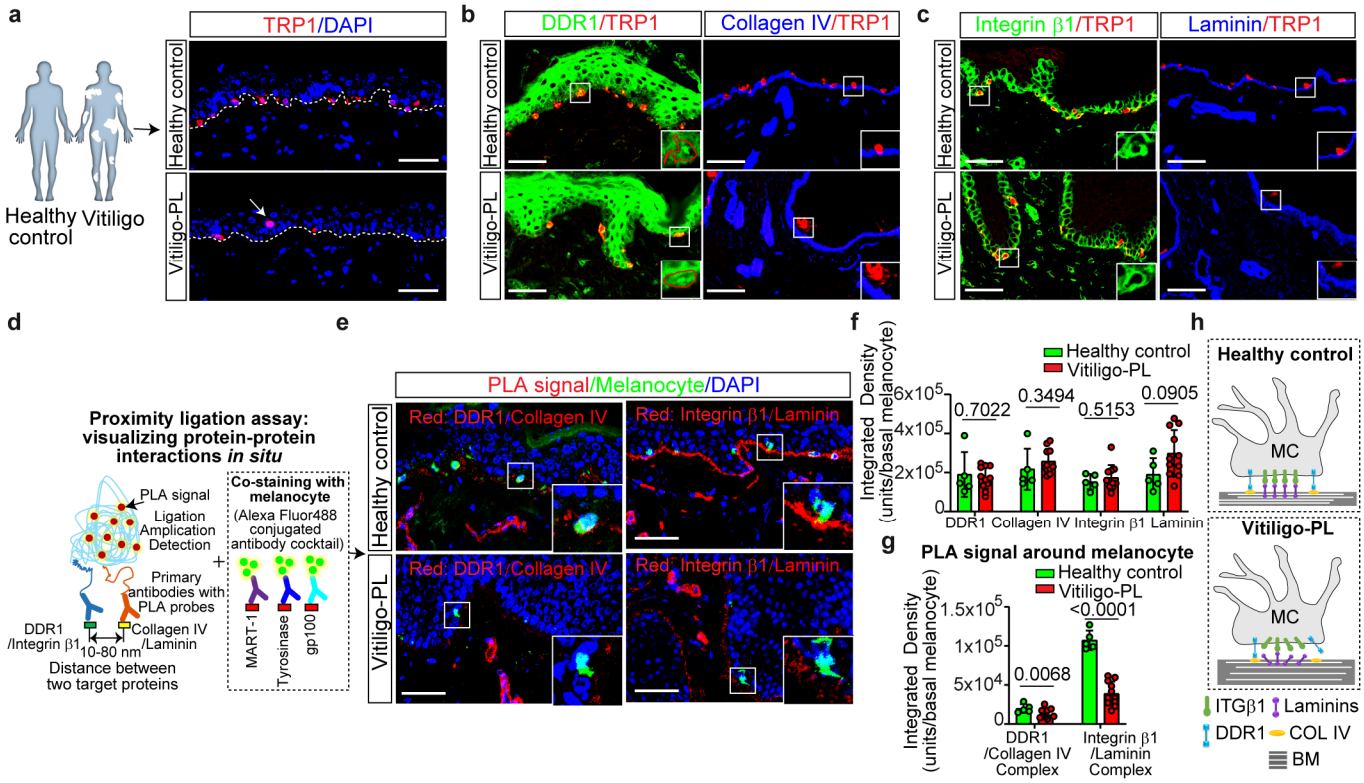

Figure 6

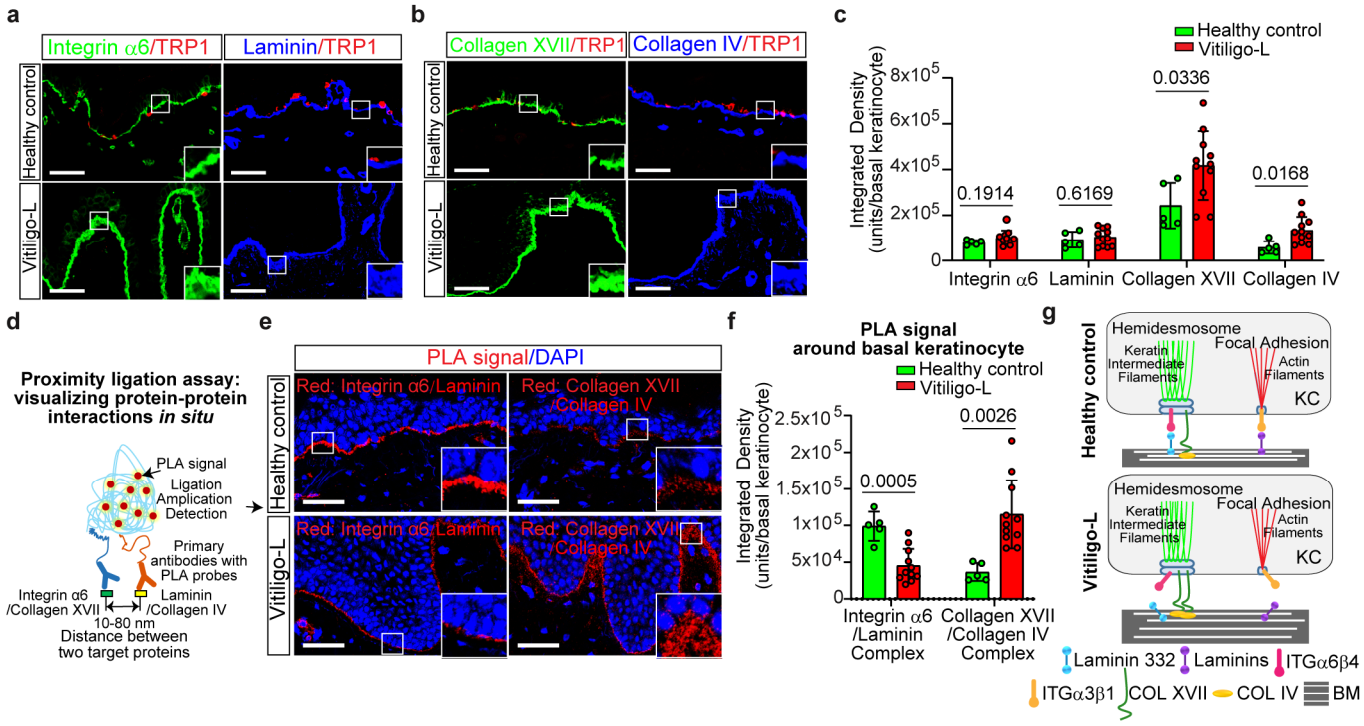

Figure 7

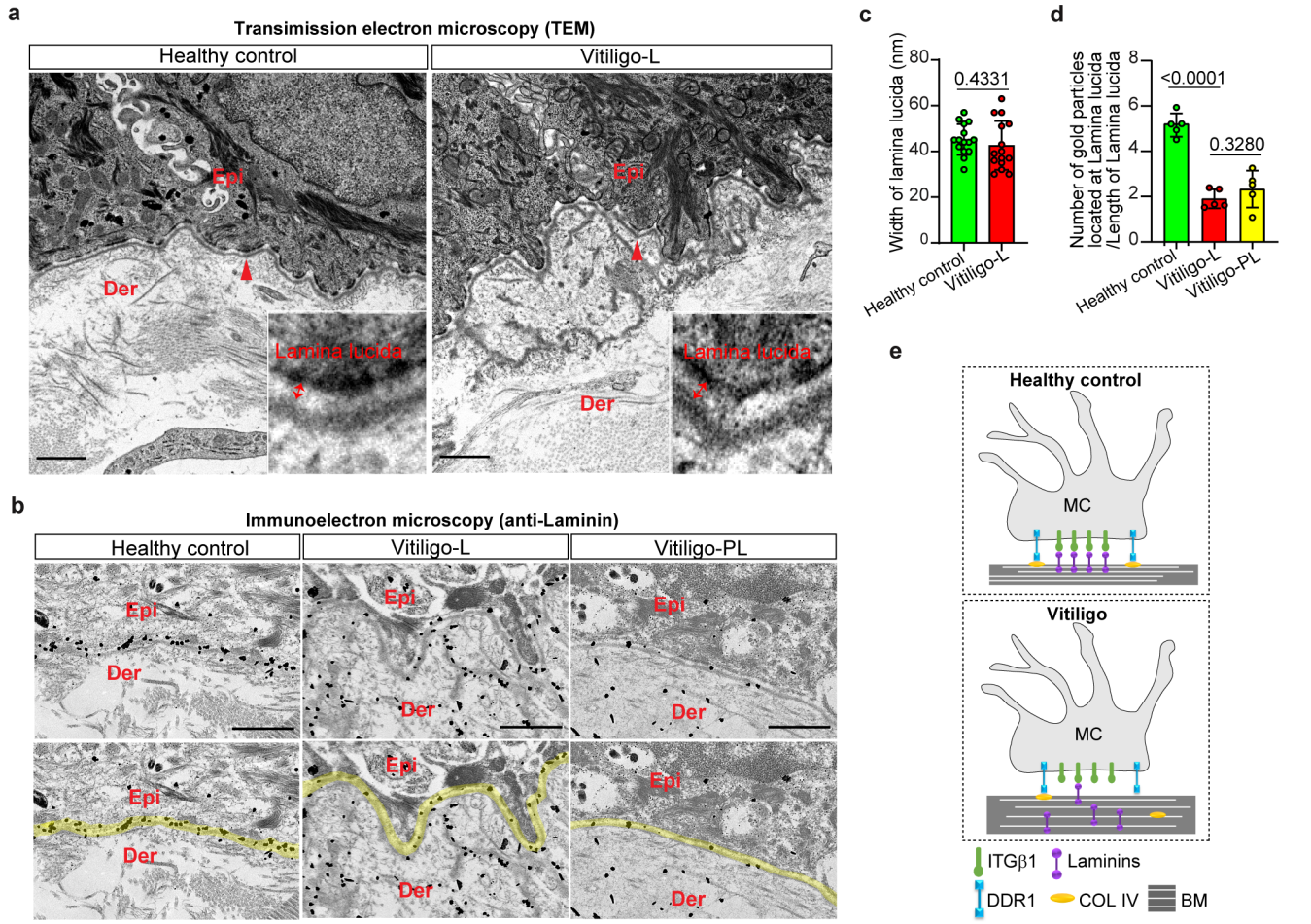

Figure 8

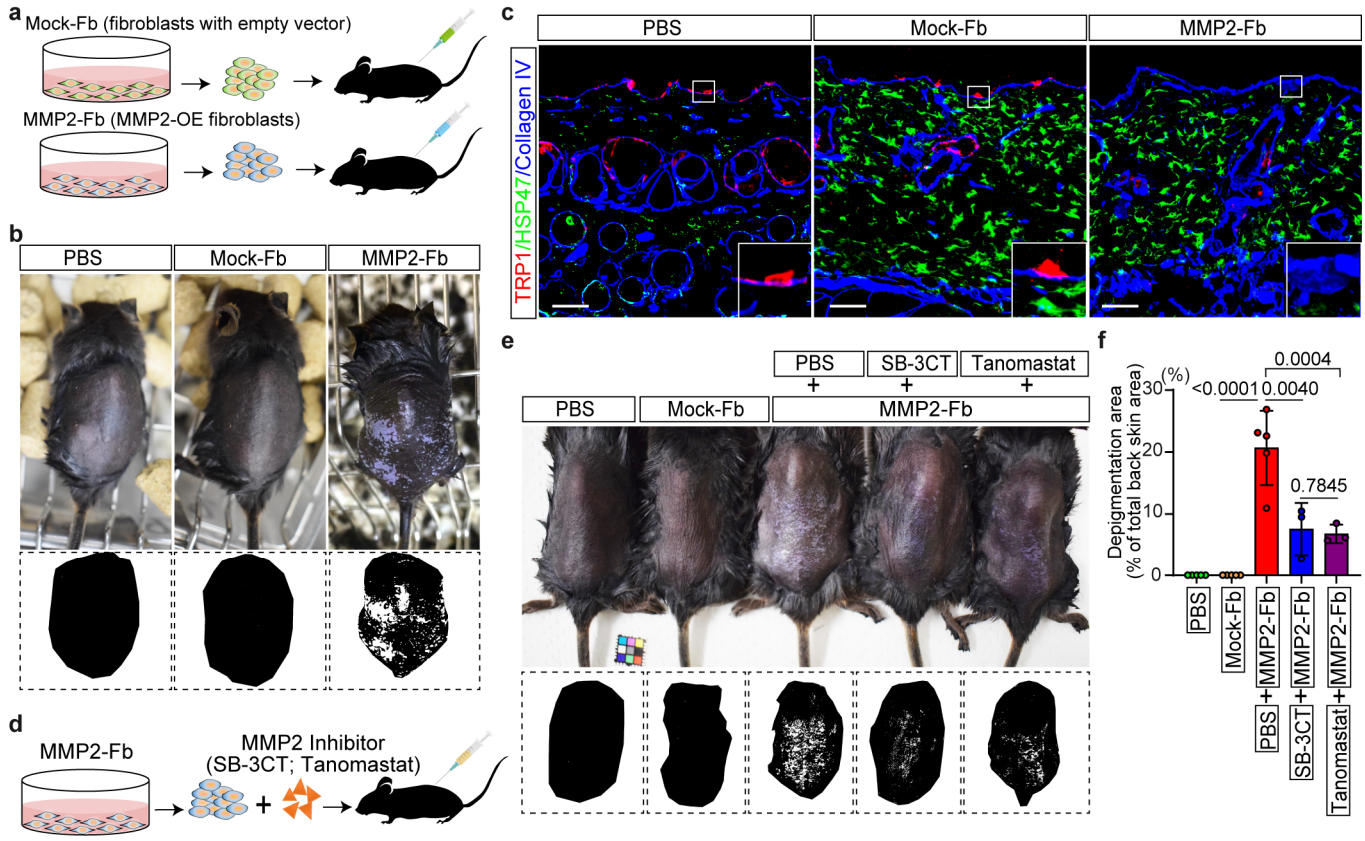

Figure 9

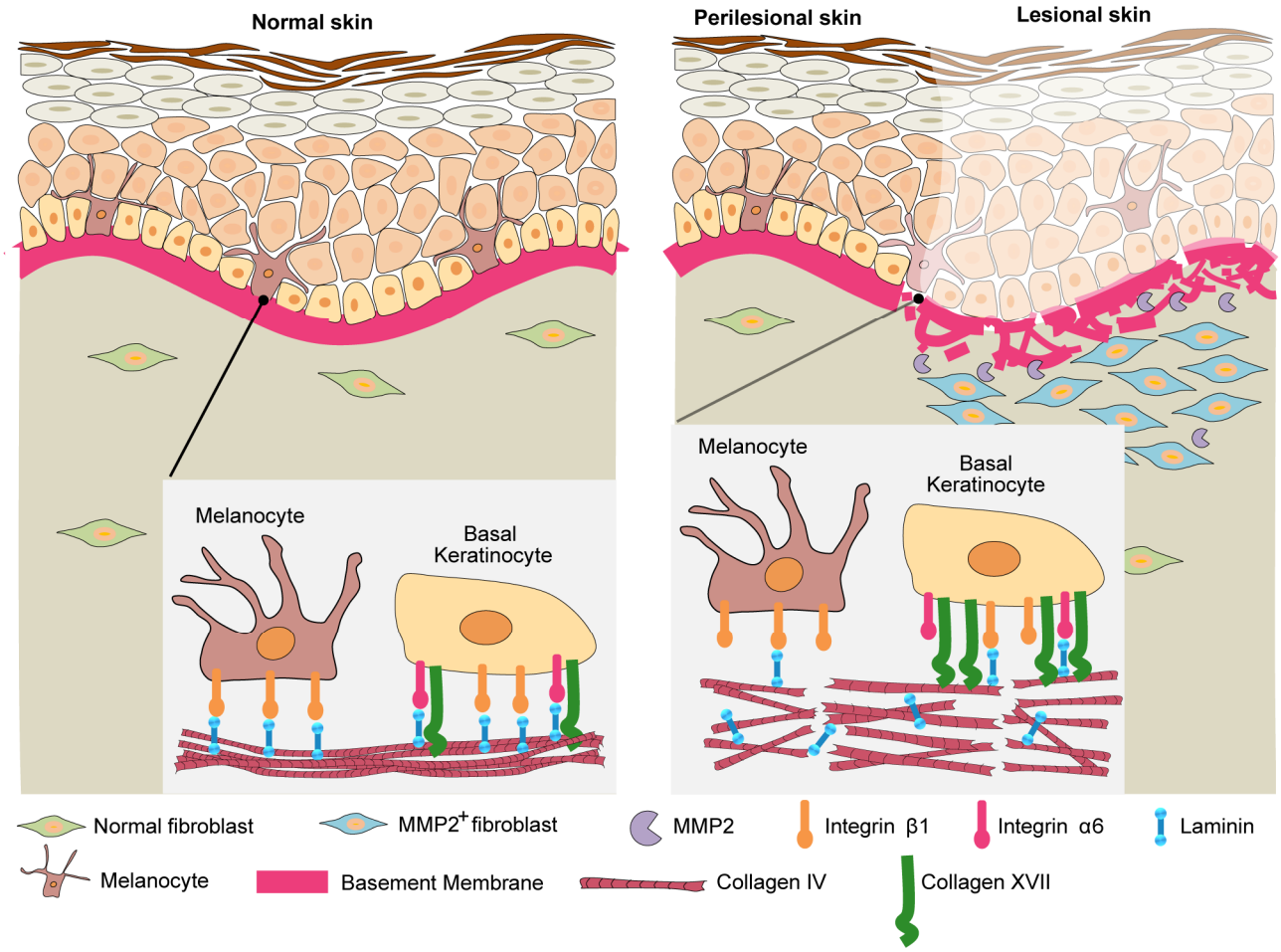
Normal skin
Perilesional skin
Lesional skin
Melanocyte
Basal Keratinocyte
Melanocyte
Basal Keratinocyte
Normal fibroblast
MMP2+ fibroblast
MMP2
Integrin β1
Integrin α6
Laminin
Melanocyte
Basement Membrane
Collagen IV
Collagen XVII

Supplementary Information

Materials & Methods

Fluorescent Immunohistochemistry Staining

Human skin tissue embedded in OCT compound (Sakura Fineteck, Tokyo, Japan) was cut into 6-μm sections for immunohistochemistry analyses. After fixation with 4% paraformaldehyde (163-20145, Wako, Osaka, Japan) for 10 min and blocking with 5% BSA for 30 min at room temperature, these sections were incubated with 1:100 diluted primary antibodies specific for TGF-β1 (ARG66427, Arigobio, Hsinchu, Taiwan), TNF-α (60291-1-Ig, Proteintech, Rosemont, USA), IL-1β (16806-1-AP, Proteintech), and IL-6 (21865-1-AP, Proteintech) and then incubated with the appropriate secondary antibody (Alex Fluor 488/555 anti-rabbit IgG, anti-mouse IgG1, anti-mouse IgG2a; 1:1,000, Invitrogen, Grand Island, NY, USA). Nuclei were counterstained with DAPI (#62248, Thermo Fischer Scientific). Slides were observed using an LSM 710 Zeiss confocal laser microscope. Images were captured using Zeiss ZEN 2012 software (Carl Zeiss Inc., Jena, Germany). Counting of positively stained cells and measurement of mean fluorescence intensity were carried out using Image J Software (NIH, http://rsb.info.nih.gov/ij/index.html).

Figure Legends

Extended Data Fig. 1. Increased cytokine expression in the epidermis of vitiliginous skin

Representative immunofluorescence staining of TGF-β1 (**a**), TNF-α (**b**), IL-1β (**c**), and IL-6 (**d**) in skin sections from healthy controls and lesional skin sections from patients with vitiligo. Nuclei were counterstained in blue with DAPI. The area in the white rectangle is shown on the lower right. Scale bars in **a, b, c**, and **d**: 50 μm.
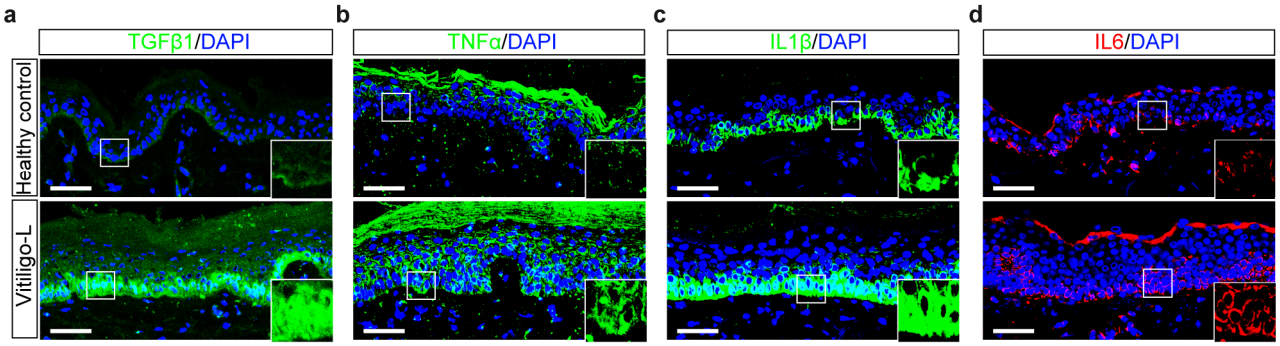
Extended Data Fig. 1